Earth and Planetary Science Letters 381 (2013) 177–187

Contents lists available at ScienceDirect

Earth and Planetary Science Letters

www.elsevier.com/locate/epsl

GPS and tectonic evidence for a diffuse plate boundary at the Azores Triple Junction

F.O. Marques [a,*], J.C. Catalão [b], C. DeMets [c], A.C.G. Costa [b,d], A. Hildenbrand [d,e]

[a] Universidade de Lisboa, Lisboa, Portugal
[b] Universidade de Lisboa, Instituto Dom Luiz, Lisboa, Portugal
[c] Department of Geoscience, University of Wisconsin–Madison, Madison, USA
[d] Université Paris-Sud, Laboratoire IDES, UMR8148, Orsay, F-91405, France
[e] CNRS, Orsay, F-91405, France

ARTICLE INFO

Article history:
Received 14 March 2013
Received in revised form 29 August 2013
Accepted 31 August 2013
Available online 25 September 2013
Editor: P. Shearer

Keywords:
GPS and structural data
plate boundary
Nubia and Eurasia
Azores Triple Junction
Terceira Rift
Mid-Atlantic Ridge (MAR)

ABSTRACT

We use GPS, bathymetric/structural, and seismic data to define the pattern of present deformation along the northern half of the Azores plateau, where the Nubia–Eurasia plate boundary terminates at the axis of the Mid-Atlantic Ridge (MAR). New and existing campaign GPS velocities from the Azores islands reveal extension oblique to a series of en échelon volcanic ridges occupied by Terceira, S. Jorge, Pico, and Faial islands. In a frame of reference defined by 69 continuous GPS stations on the Eurasia plate, Terceira Island moves 2 ± 1 mm/yr away from Eurasia, consistent with the island's location within the Terceira Rift and plate boundary structure. The volcanic ridges south of the Terceira Rift move toward WSW at progressively faster rates, reaching a maximum of 3.5 ± 0.5 mm/yr (2-σ) for the Pico/Faial volcanic ridge. The hypothesis that the Terceira Rift accommodates all Nubia–Eurasia plate motion is rejected at high confidence level based on the motions of sites on S. Jorge Island just west of Terceira Rift. All of the islands move relative to the Nubia plate, with Pico Island exhibiting the slowest motion, only 1 ± 0.5 mm/yr (2-σ). Detailed bathymetry from the interior of the hypothesized Azores microplate reveals faults that crosscut young MAR seafloor fabric. These observations and the GPS evidence for distributed deformation described above argue against the existence of a rigid or semi-rigid Azores microplate, and instead suggest that Nubia–Eurasia plate motion is accommodated by extension across a ~140-km-wide zone east of the MAR axis, most likely bounded to the north by the northern shoulder of the Terceira Rift. The MAR spreading rate along the western end of the Azores deformation zone (~38.5°N–39.5°N) is intermediate between the Eurasia–North America rate measured at 39.5°N and the Nubia–North America rate measured at 38.5°N, consistent with the joint conclusions that the Nubia–Eurasia boundary is broad where it intersects the MAR, and the Azores Triple Junction is diffuse rather than discrete.

1. Introduction

The Azores Triple Junction is located at the western end of the Nubia–Eurasia plate boundary, where the North America, Eurasia and Nubia plates meet (Fig. 1). Although its existence has long been recognized, there is as yet no consensus regarding its location and the nature of deformation in the vicinity of the triple junction (e.g. Krause and Watkins, 1970; Searle, 1980; Miranda et al., 1991; Luís et al., 1994; Lourenço et al., 1998; Luís and Miranda, 2008). The triple junction is marked by a ~15% decrease in MAR seafloor spreading rates from 39.5°N, where Eurasia–North America motion occurs, to ~38.5°N, where Nubia–North America plate motion occurs (DeMets et al., 2010). Along the ~100-km-long stretch of the ridge between ~38.5°N and 39.5°N, the average seafloor spreading rate is intermediate between that for Eurasia–North America and Nubia–North America motion (DeMets et al., 2010), suggesting that either a rigid or nearly rigid Azores microplate rotates independently east of the MAR axis between ~38.5°N and 39.5°N, or that distributed deformation occurs across a ~140-km-wide zone east of the MAR axis.

In this study, we present and interpret GPS observations from sites in the Azores archipelago in the context of existing bathymetric/structural and seismic data to address three fundamental questions related to the Azores Triple Junction: (1) Is the Nubia–Eurasia plate boundary discrete or diffuse near the Azores Triple Junction and, by implication, is the triple junction discrete or diffuse? (2) Where is the present Nubia–Eurasia plate boundary in this region? (3) Is there an Azores microplate? Previous authors have used a variety of data to address some of these questions, including seafloor spreading magnetic lineations (e.g. Krause and Watkins, 1970; Searle, 1980; Luís et al., 1994; Luís and Mi-

* Corresponding author. Tel.: +351 217500000; fax: +351 217500064.
E-mail address: fomarques@fc.ul.pt (F.O. Marques).

0012-821X/$ – see front matter
http://dx.doi.org/10.1016/j.epsl.2013.08.051

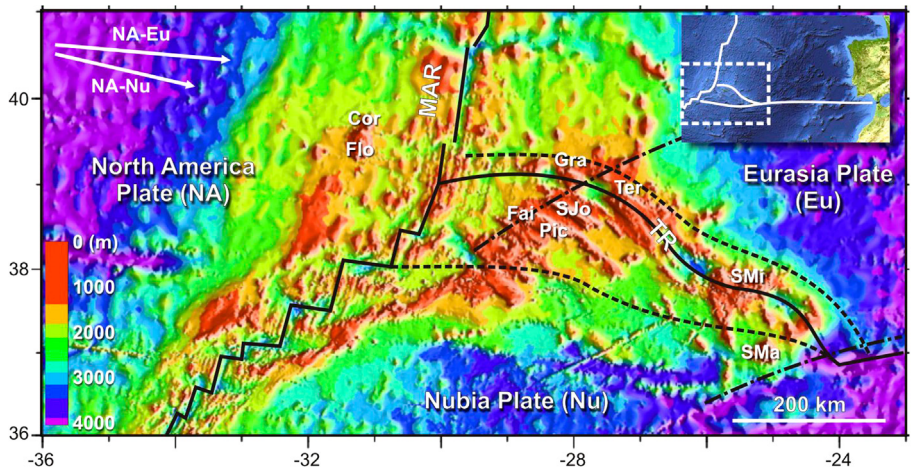

Fig. 1. Sketch illustrating the tectonic setting of the Azores Triple Junction. Inset on top right corner for location. Inset on top left corner for the kinematics of the Nubia and Eurasia lithospheric plates (DeMets et al., 2010). Dashed lines mark the boundaries of a hypothetical Azores microplate. Dash-dotted lines represent small circles around the MORVEL Nubia–Eurasia pole. The nine Azores islands are, from W to E, Corvo (Cor), Flores (Flo), Faial (Fai), Pico (Pic), S. Jorge (SJo), Graciosa (Gra), Terceira (Ter), S. Miguel (SMi), and Santa Maria (SMa).

randa, 2008), SONAR and marine bathymetry (e.g. Searle, 1980; Madeira and Ribeiro, 1990; Lourenço et al., 1998), bathymetric and seismic observations (Borges et al., 2007), and GPS (Fernandes et al., 2006). A key goal of this paper is to use a critical subset of observations to evaluate and refine the emerging view that Nubia–Eurasia plate motion is accommodated by deformation distributed across the northern half of the Azores plateau.

This paper is organized as follows. We first present and analyze the GPS observations that are the core of the study, including descriptions of newly estimated Nubia and Eurasia plate angular velocities in the ITRF2008 reference frame, and the resulting Nubia–Eurasia relative angular velocity. We next describe relevant bathymetric observations and the information they suggest about the character and location of regional deformation, albeit over time scales significantly longer than for the GPS observations. Finally, we discuss the implications of the GPS velocity field in the context of bathymetric/structural observations and seismic data.

2. GPS data

The GPS observations used in this study consist of the following: (1) new measurements at 35 campaign sites on Faial, Pico and Terceira islands (shown by red circles in Fig. 2A), (2) measurements at 117 continuous sites on the Nubia and Eurasia plates (Figs. 3 and 4), and (3) velocities for 15 GPS stations on S. Jorge Island from Mendes et al. (2013). Procedures for processing the new campaign and continuous data are described below.

2.1. Campaign GPS data

The Azores central group GPS geodetic–geodynamic network was established in 2001 in the aim of STAMINA and SARAZORES projects (Navarro et al., 2003; Catalão et al., 2006). It consists of 35 rock-anchored benchmarks on Faial, Pico and Terceira islands (14, 8 and 13 marks, respectively), with an average spacing of 5 km (Fig. 2A).

The principal data used for this study, from 35 stations on Faial, Pico and Terceira islands (locations shown in Fig. 2A and listed in Table 1), were acquired during seven surveys from 2001 to 2013. During each survey, every benchmark was occupied for two-to-four 24 h sessions with a sampling rate of 30 s and elevation mask of 15°. During each survey, at least six stations were observed simultaneously and one station per island was measuring continuously (FAIM for Faial, TOMA for Terceira and PPIL for Pico). For this

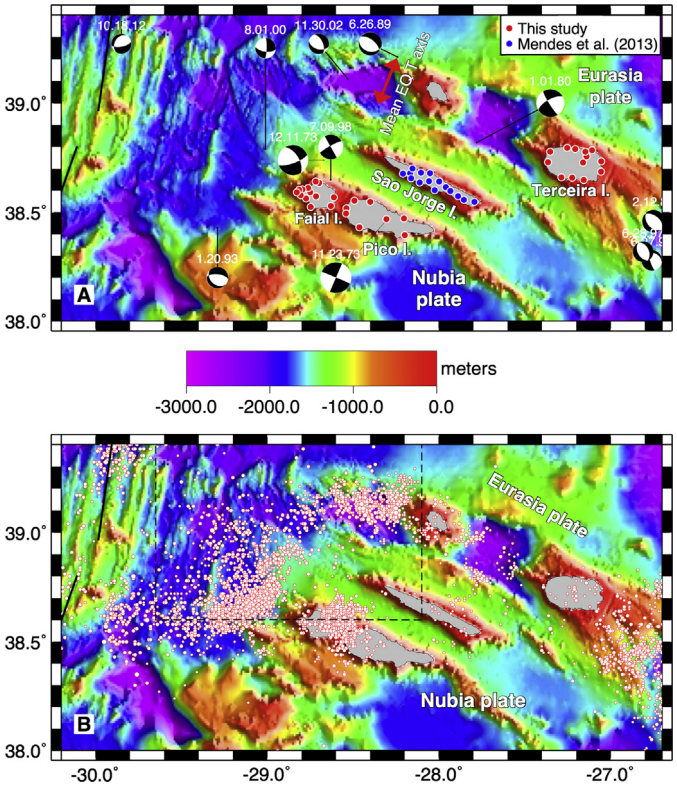

Fig. 2. A – locations of GPS sites used for this study and earthquake focal mechanisms for the study area. Bathymetry is a 1-km-resolution grid from J. Luis (http://w3.ualg.pt/~jluis/misc/ac_plateau1km.grd). Legend indicates source of the GPS velocities for Faial, Pico, S. Jorge and Terceira islands. Earthquake focal mechanisms are from the global centroid-moment tensor catalogue (Dziewonski et al., 1981; Ekstrom et al., 2012) and Borges et al. (2007 – labeled 11.23.73 and 12.11.73). Double-headed red arrow shows the average tension axis direction for the focal mechanisms of earthquakes in the diffuse deformation zone (29.5°W–27.5°W). B – epicentres of M > 1 earthquakes for the period 1998–2013, from the Portuguese IPMA catalogue, scaled by magnitude. Dashed rectangle indicates the region shown in Fig. 6. (For interpretation of the references to color in this figure legend, the reader is referred to the web version of this article.)

12-yr-long time series, each station was visited at least four times and observed for at least eight 24-h sessions.

GPS phase observations were analyzed using GAMIT software version 10.4 (Herring et al., 2010). The processing and analysis were made in two-step approach according to Dong et al. (1998).

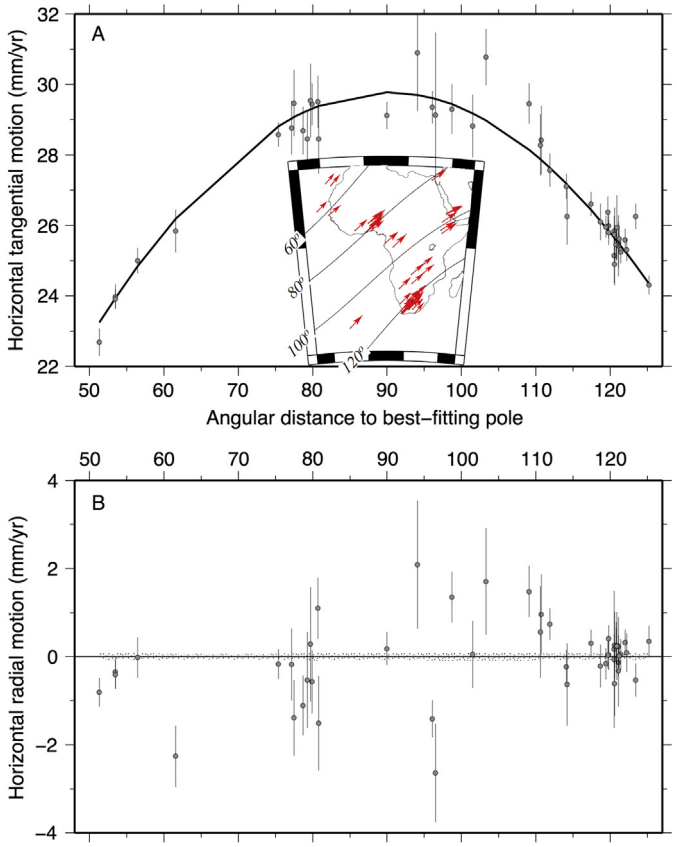

Fig. 3. Locations (map inset) and velocity components of 49 Nubia plate GPS sites used to estimate the instantaneous Nubia plate angular velocity relative to ITRF2008. Red arrows in map inset show GPS site velocities in ITRF2008. A – component of GPS station velocities parallel to small circles around the best-fitting Nubia-ITRF2008 pole. B – component of GPS station velocities orthogonal (radial) to small circles around the best-fitting pole. Vertical bars indicate 1-σ rate uncertainties. Stippled pattern shows 1-σ uncertainty in the predicted rates propagated from the angular velocity covariances. (For interpretation of the references to color in this figure legend, the reader is referred to the web version of this article.)

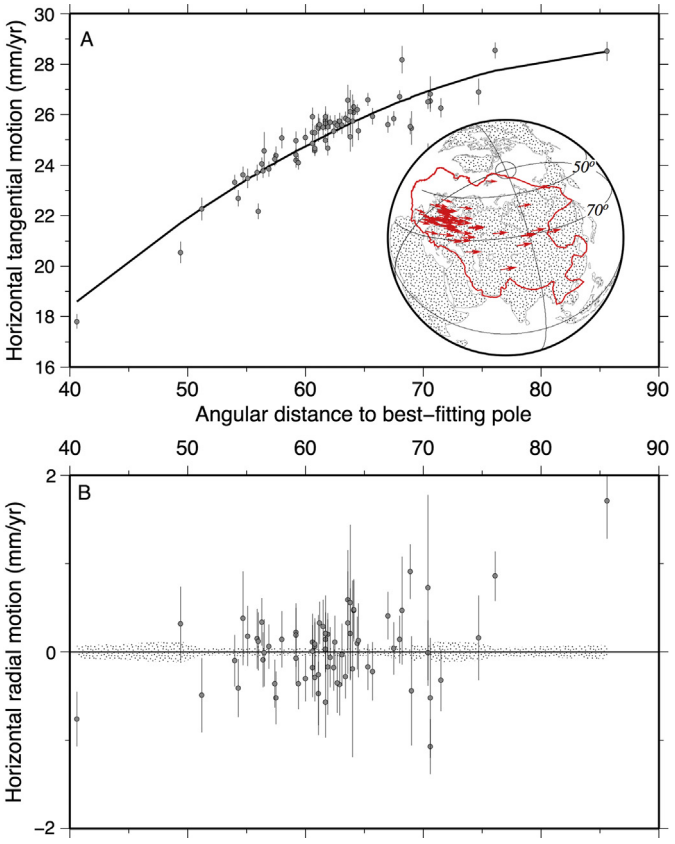

Fig. 4. Locations (map inset) and velocity components of 69 Eurasia plate GPS sites used to estimate the instantaneous Eurasia plate angular velocity relative to ITRF2008. Red arrows in map inset show GPS site velocities in ITRF2008. A – component of GPS station velocities parallel to small circles around the best-fitting Eurasia-ITRF2008 pole. B – component of GPS station velocities orthogonal (radial) to small circles around the best-fitting pole. Vertical bars indicate 1-σ rate uncertainties. Stippled pattern shows 1-σ uncertainty in the predicted rates propagated from the angular velocity covariances.

First, GPS phase observations from each day were used to estimate loosely constrained station coordinates, tropospheric zenith delay parameters and orbital and earth orientation parameters and associated variance–covariance matrices. We have included in the analysis 117 IGS continuous operating GPS stations in order to tie the regional measurements to a global reference frame. We have selected IGS stations distributed worldwide and stations from EUREF network. The GAMIT solution was computed using loose constraints on the *a priori* station coordinate (0.5 m), *a priori* hydrostatic and wet models from Saastamoinen (1972a, 1972b, 1973) and Global Mapping Functions (Böhm et al., 2006), solid earth tides according to IERS conventions (Petit and Luzum, 2010), ocean tidal loading from the FES2004 ocean tide model (Lyard et al., 2006) and receiver and satellite antenna phase centre corrections were modeled with IGS08 ANTEX files from IGS. We used SOPAC's final orbits generated under the scope of the IGS reprocessing analysis and coordinates for all the stations expressed in the ITRF2005 (Altamimi et al., 2007).

Following analysis of the raw GPS data, daily GAMIT solutions were used as quasi-observations in GLOBK to obtain position time series for all sites. In this solution, the regional daily solutions were combined with global daily solution from the IGS1, IGS2, IGS3 and EURA networks computed by SOPAC, the h-files (GAMIT interchange format). Position time series were analyzed to detect and remove outliers and detect possible vertical offsets caused by erroneous antenna height. After editing, site coordinates and velocities were estimated with respect to ITRF2008 reference frame from *a priori* values of coordinates and velocities of IGS permanent sites.

A second iteration of this process was made using GLOBK estimated coordinates and velocities as *a priori* in GAMIT, now with a constraint of 5 cm for coordinates of the surveyed sites. The final solution of site coordinates and velocities was computed by GLOBK using generalized constraints by minimizing the velocity for a large number of IGS stations and estimating a Helmert transformation. The ITRF2008 reference frame was adopted in this last step. The final solution combines seven survey-mode GPS campaigns with IGS stations globally between 2001 and 2013. The weighted RMS of the residual velocity for sites used to define the reference frame (IGS sites) are 0.78, 0.66, 1.2 mm/yr for east, north and vertical components, respectively. Table 1 gives the estimated velocities and formal 1-σ uncertainties for GPS sites on Faial, Pico, and Terceira islands. The campaign velocity uncertainties are the formal errors derived from a weighted linear regression of each station time series. They depend on the time spanned by the observations as well as the number of site occupations and estimated location uncertainties.

The velocities for all campaign GPS sites on S. Jorge Island were taken from Mendes et al. (2013), who process their campaign GPS data with GAMIT using procedures the same as those outlined above (including the underlying geodetic reference frame ITRF2008). By implication, their velocities can be included with ours without concerns about inconsistencies between the two.

Table 1
GPS site velocities and 1-σ uncertainties (units mm/yr).

	Long.	Lat.	ve	vn	1-σ-ve	1-σ-vn
PRIB	331.801	38.39558	11.46	14.43	0.15	0.16
PPRN	331.796	38.47172	10.82	14.3	0.11	0.13
PBJQ	331.695	38.46891	11.47	14.77	0.10	0.11
PSLU	331.601	38.54895	11.15	15.14	0.14	0.16
PSMT	331.536	38.4324	11.6	14.69	0.11	0.12
PDRO	331.507	38.55444	11.28	14.75	0.12	0.13
PMAD	331.461	38.51932	11.46	14.86	0.09	0.1
PCAL	331.460	38.49515	11.24	15.02	0.12	0.13
TPVT	332.945	38.73359	12.91	16.15	0.16	0.19
TPOM	332.944	38.68715	13.27	15.07	0.12	0.14
TCAP	332.892	38.78465	12.19	15.56	0.11	0.12
TSBR	332.860	38.75664	12.37	15.6	0.14	0.17
TCAB	332.854	38.77781	13.15	14.84	0.11	0.12
TSER	332.843	38.64884	12.27	16.22	0.18	0.22
TGOL	332.839	38.72859	13.01	16.04	0.14	0.16
TQRB	332.793	38.78996	14.06	14.65	0.13	0.14
TOMA	332.776	38.65864	13.02	17.31	0.09	0.09
TBIS	332.747	38.79645	14.5	13.77	0.10	0.11
TCCD	332.713	38.6611	13.46	16.51	0.10	0.11
TRAM	332.648	38.77842	15.57	14.79	0.16	0.20
TPTE	332.635	38.73034	14.36	15.67	0.16	0.18
FFAR	331.398	38.59532	13.2	14.74	0.14	0.16
FPMG	331.388	38.56857	11.99	15.3	0.20	0.22
FAIM	331.371	38.52952	11.42	14.89	0.09	0.10
FCDR	331.303	38.63617	12.53	15.83	0.15	0.16
FCGO	331.285	38.57371	11.4	14.12	0.15	0.17
FPN2	331.282	38.6417	12.29	15.34	0.16	0.18
FCBR	331.253	38.52527	11.55	14.55	0.20	0.22
FPCD	331.250	38.59254	11.3	15.57	0.16	0.18
FFAJ	331.238	38.61159	11.1	14.88	0.15	0.16
FVAR	331.226	38.56446	11.96	15.98	0.12	0.14
FPDN	331.206	38.60598	11.55	15.13	0.23	0.27
FVUS	331.195	38.57873	12.43	16.37	0.23	0.26
FVUN	331.186	38.60447	12.1	15.24	0.14	0.16
FVUL	331.172	38.59247	12.65	16.11	0.21	0.23

2.2. Continuous GPS data for the Nubia and Eurasia plates

All of the continuous GPS data we used from sites on the Nubia and Eurasia plates are in the public domain and were procured variously from EUREF (epncb.oma.be), NGS (geodesy.noaa.gov/CORS), SOPAC (www.sopac.ucsd.edu), TRIGNET (trignet.co.za), and UNAVCO (unavco.org). The raw GPS data were processed with release 6.1 of the GIPSY software suite from the Jet Propulsion Laboratory (JPL). No-fiducial daily GPS station coordinates were estimated using a precise point-positioning strategy (Zumberge et al., 1997), including constraints on *a priori* tropospheric hydrostatic and wet delays from Vienna Mapping Function (VMF1) parameters (http://ggosatm.hg.tuwien.ac.at), elevation- and azimuthally-dependent GPS and satellite antenna phase centre corrections from IGS08 ANTEX files (available via ftp from sideshow.jpl.nasa.gov), and corrections for ocean tidal loading (http://holt.oso.chalmers.se). Phase ambiguities were resolved using GIPSY's single-station ambiguity resolution feature. Daily no-fiducial station location estimates were transformed to IGS08, which conforms to ITRF2008 (Altamimi et al., 2011), using daily seven-parameter Helmert transformations from JPL. We assume that the geocentre as defined in ITRF2008 is stable and make no correction for possible geocentral motion (Argus, 2007).

In light of compelling evidence that noise in the estimates of daily station coordinates remains strongly correlated out to inter-station distances of 3000 km (Marquez-Azua and DeMets, 2003), we used a straightforward method outlined by these authors to estimate and reduce spatially correlated noise between GPS sites. Interested readers are referred to Marquez-Azua and DeMets (2003) and references therein for details.

Prior to correcting any of our 119 GPS time series for spatially-correlated noise, their 1-σ daily repeatabilities were 1.8 mm in both the northing and easting components. Time-correlated noise had average amplitudes of 4.4 mm and 4.5 mm in the north and east components. After correcting each time series for their spatially correlated noise, the average daily coordinate repeatability was reduced to 1.5 mm in both horizontal components and 3.5 mm and 3.7 mm in the northing and easting components of the time-correlated noise. Corrections for the common-mode noise thus effected ~20% reductions in the noise, which reduce the uncertainties in the site velocities described next.

Uncertainties in the velocities of the continuous GPS sites were estimated using an expression from Mao et al. (1999) that relates the velocity uncertainty to the length of a GPS station's time series, the number of time series measurements, and the magnitudes of the white, flicker, and random-walk noise per site. We approximated the respective amplitudes of the white and time-correlated noise at each site from the WRMS scatter of a site's daily locations relative to its monthly-average locations and the average amplitude of longer-period noise manifested in the site's coordinate time series. We assigned an average value of 1 mm/yr for the magnitude of the random-walk noise. Using this algorithm, the standard errors in the 119 continuous site velocities ranged from ±0.24 mm/yr to ±2 mm/yr for time series that span 2 yr to 19 yr. Inversions of the GPS velocities using these uncertainties (see below) return values of reduced chi-square (i.e. chi-square per degree of freedom) of 1.5 and 2.2, suggesting that the estimated uncertainties may be modestly underestimated (20–50%).

2.3. Motion of Nubia relative to ITRF2008

We determined the angular velocity for the Nubia plate relative to ITRF2008 (Table 2) from an inversion of the velocities of 49 stations (Fig. 3) west of the East Africa Rift (see map inset for Fig. 3) in nominally stable parts of the plate interior. The Nubia site velocities span a large angular distance with respect to their best-fitting pole (Fig. 3) and thus impose strong geometric constraints on both the pole location and angular rotation rate. The components of the 49 site velocities around the pole (tangential

Table 2
GPS angular velocities.

Plate pair	Angular velocity (ω)			Angular velocity covariances (σ)						
	Latitude (°N)	Longitude (°E)	ω (°/Myr)	Sites	σ_{xx}	σ_{yy}	σ_{zz}	σ_{xy}	σ_{xz}	σ_{yz}
EU-ITRF08	54.5	−99.1	0.257	69	2.67	0.52	3.92	0.56	2.83	0.72
NU-ITRF08	49.1	−80.8	0.268	49	4.37	1.36	1.58	0.96	−1.20	−0.43
NU-EU	−6.8	−26.5	0.058	118	7.08	1.88	5.55	1.53	1.67	0.30
NU-EU (1)	21.6	−20.4	0.131							
NU-EU (2)	−10.3	−27.7	0.103							
NU-EU (3)	−7.5	−21.1	0.061							
NU-EU (4)	−8.1	−19.8	0.053							

Angular velocities describe counter clockwise rotation of the first plate relative to second. NU is Nubia plate; EU is Eurasia plate. Covariance units are 10^{-10} rad^2/Myr^2. Nubia–Eurasia angular velocities are as follows: (1) MORVEL – DeMets et al. (2010); (2) Calais et al. (2003); (3) Argus et al. (2010); (4) Altamimi et al. (2011).

component) and radial to the pole are well described by the best-fitting angular velocity (Fig. 3) and have a weighted RMS misfit of only 0.75 mm/yr. The GPS velocities are thus consistent with the hypothesis that the interior of the Nubia plate deforms slowly or not at all. Reduced chi-square for the 49 Nubia sites is 1.46, close to the value of 1.0 expected if the plate is not deforming and the GPS velocity uncertainties are approximately correct.

2.4. Motion of Eurasia relative to ITRF2008

The angular velocity for the Eurasia plate relative to ITRF2008 (Table 2) was determined from an inversion of the velocities of 69 stations (Fig. 4). The sites are distributed throughout the plate interior, but are heavily weighted toward European stations. Stations from Fennoscandia are excluded due to significant isostatic rebound in these areas (Nocquet et al., 2005). The components of the 69 site velocities around the pole (tangential component) and radial to the pole are well described by the best-fitting angular velocity (Fig. 4) and have a weighted RMS misfit of only 0.68 mm/yr, similar to that for the Nubia plate and consistent with little or no deformation within the areas of the Eurasia plate that are sampled by the 69 GPS sites. Reduced chi-square for the 29 Eurasia sites is 2.2, ∼50% larger than expected if the GPS velocity uncertainties were correct. Roughly half of the larger-than-expected misfit is attributable to three poorly fit velocities for GPS sites in NE Asia. Including or omitting these three site velocities has little impact on the resulting best-fitting angular velocity – we thus elected to use these three velocities.

2.5. Motion of Nubia relative to Eurasia

A simultaneous inversion of all 119 Eurasia and Nubia plate GPS velocities gives a best-fitting angular velocity for Nubia relative to Eurasia (Table 2) that lies ∼3000 km south of the MORVEL geologically-estimated Nubia–Eurasia pole (Table 2 and DeMets et al., 2010), but agrees well with poles estimated by other authors from GPS measurements on these two plates (Table 2). Despite the large difference between pole locations determined from GPS and that of the MORVEL geologic model, their respective angular velocities predict similar motions near the centre of the study area (Fig. 5C). Our new GPS-based angular velocity predicts that Nubia moves 4.6 ± 0.3 mm/yr toward S87.9°W $\pm$ 3.3° (95% uncertainties) relative to Eurasia. For comparison, MORVEL predicts 4.5 ± 0.4 mm/yr toward S68.1°W $\pm$ 2.8°. The difference in the predicted velocities is too small to affect any of the conclusions we reach below.

3. GPS velocity fields for Faial, Pico, S. Jorge and Terceira islands

3.1. GAMIT/GIPSY velocity field combination and velocity uncertainties

In order to evaluate the consistency of our velocity solutions from GAMIT and GIPSY, we compared the ITRF2008 velocities of 32 globally-distributed IGS stations for which we processed continuous data with both software packages. On average, the Cartesian components of the 32 station velocities differ by only −0.23, 0.17, and −0.17 mm/yr for the X, Y and Z velocity components, respectively. The close agreement between the two velocity solutions validates our respective processing methodologies and our separate realizations of the station velocities in ITRF08. From 38 continuous stations common to both analyses, we estimated and applied translational and rotational parameters to transform the GAMIT velocity solution onto the GIPSY solution. This altered the GAMIT velocities in the study area by only 0.07 mm/yr and 0.12 mm/yr in the east and north velocity components, reflecting the high degree of consistency in the solutions prior to their formal combination.

Whereas the uncertainties in the continuous GPS site velocities were estimated using a method that accounts for non-random sources of noise in GPS time series (described above), estimating realistic uncertainties for campaign site velocities is more difficult since the noise characteristics of campaign sites are poorly known. White-noise-only models, as assumed in estimating velocity uncertainties via standard linear regressions of station position time series, may underestimate velocity uncertainties by a factor of 5 to 11 (Mao et al., 1999). To approximate realistic velocity uncertainties at the campaign sites, we first determined formal velocity uncertainties via standard weighted linear regressions of the station coordinate time series. The formal uncertainties were typically ± 0.1 to ± 0.2 mm/yr, smaller than the velocity uncertainties for continuous sites with comparable time spans. We therefore increased the formal velocity uncertainties for the campaign sites by a factor of three, such that the adjusted velocity uncertainties were larger than for continuous GPS sites with comparable observation time spans (∼10 yr). Given the subjective nature of this adjustment, we also repeated the kinematic tests described below while using campaign velocity uncertainties that were increased by a factor of four. Using these more conservative error estimates did not however significantly alter any of the results or conclusions presented below.

3.2. Island motions relative to Nubia and Eurasia plates and the Pico–Faial volcanic ridge

In order to test a variety of hypotheses related to deformation in the Azores, we analyzed the campaign site velocities in three frames of reference, one fixed to the Eurasia plate (Figs. 5 C and D), one fixed to a frame of reference that minimizes the motion of stations on Pico and eastern Faial islands (Fig. 5a), and one fixed to the Nubia plate (not shown, but discussed below). The results for Terceira, S. Jorge, and Pico and Faial islands are described below. Note that Pico and Faial islands occupy the same volcanic ridge.

3.3. Terceira Island

The 13 GPS sites on Terceira Island move systematically faster to the west than predicted by the Eurasia plate angular velocity (Fig. 5C), at rates that vary between 1 and 2.8 mm/yr (Fig. 5D). The average rate near the centre of the island, 2 ± 1 mm/yr (2-σ), is nearly half of the Nubia–Eurasia rate at this location (Fig. 5d), consistent with the island's location inside the Terceira Rift and along the plate boundary (Fig. 2). Further discussion of this velocity field and its implications for the volcanotectonics of Terceira Island and vicinity will be presented in a future paper.

We tested for statistically significant motion of Terceira Island relative to the Eurasia plate using the Stein and Gordon (1984) test for an additional plate boundary, as follows: separate inversions of the 69 Eurasia plate site velocities and 13 Terceira site velocities were used to estimate best-fitting angular velocities and least-squares misfits for the Eurasia plate and an independently moving Terceira Island. A simultaneous inversion of all 82 velocities was used to a single angular velocity to describe Eurasia plate motion including Terceira Island. We then use the F-ratio test to evaluate whether the former, two-plate model improves the fit significantly relative to the latter one-plate model. The outcome, $F = 21.5$ for 3 versus 158 degrees of freedom, indicates that the one-plate model degrades the fit at high confidence level (much greater than 99%). The kinematic evidence thus strongly supports significant motion of Terceira Island relative to the Eurasia plate.

3.4. S. Jorge Island

On average, the 15 S. Jorge GPS sites move WSW away from the Eurasia plate at 2.7 ± 0.7 mm/yr (2-σ) (Figs. 5 B and C) and

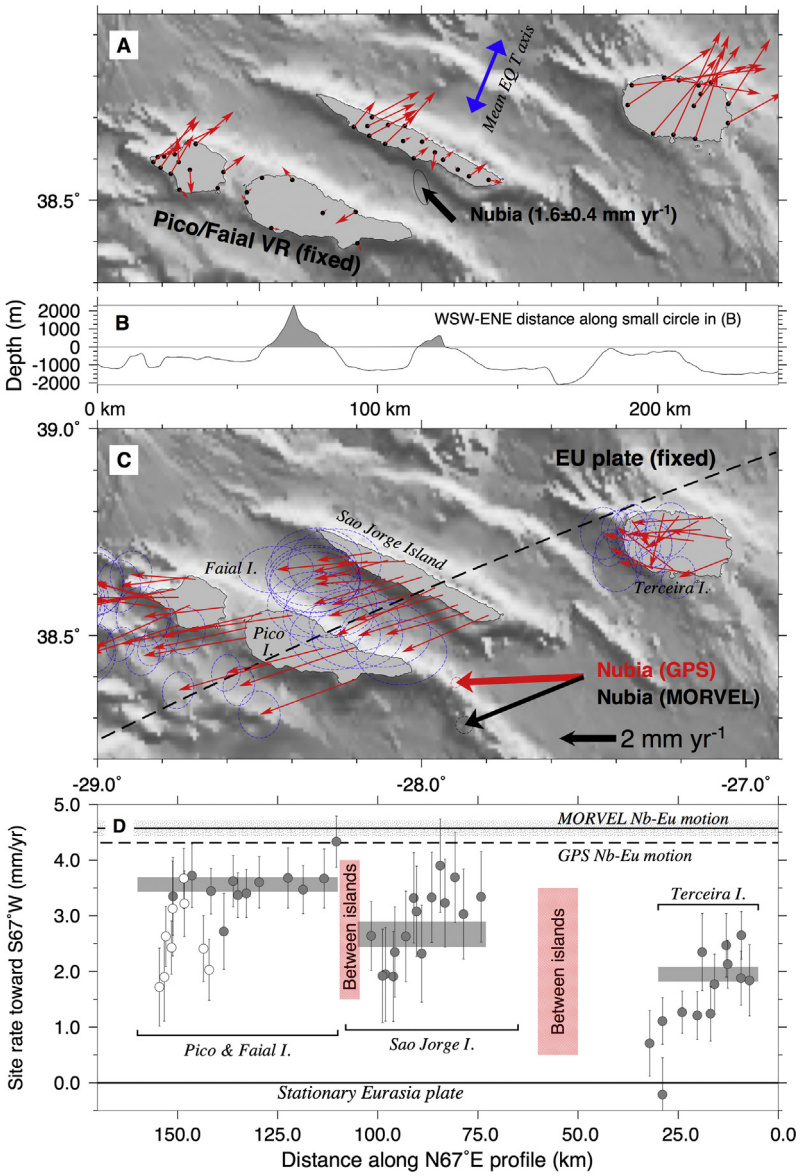

Fig. 5. A: GPS site velocities (red arrows) and Nubia plate motion (black arrow with 1-σ uncertainty) relative to Pico/Faial volcanic ridge (VR). Black arrow gives the scale. Velocity error ellipses are omitted for clarity. Blue arrow indicates mean tensional axis for eight earthquakes shown in Fig. 2A (see text). B: Topography and bathymetry along the dashed line in Part C. C: GPS site velocities (red arrows) relative to Eurasia plate. Bold red and black arrows show Nubia plate motion predicted by the best-fitting GPS-derived Nubia–Eurasia angular velocity (Table 1) and MORVEL (DeMets et al., 2010). Blue velocity error ellipses are 1-σ. D: GPS site velocities collapsed onto a WSE-ENE transect of the islands (indicated by dashed line in C). Circles show site velocities from Panel B rotated onto N67°E, the Nubia–Eurasia plate slip direction predicted by MORVEL in the study area. Error bars are 1-σ. Sites on Terceira Island move ~1 mm/yr with respect to the Eurasia plate. Grey bars show weighted average rates and formal 1-σ uncertainties. Open circles show site velocities on Faial Island possibly biased by recent volcanic deformation. (For interpretation of the references to color in this figure legend, the reader is referred to the web version of this article.)

~1 mm/yr to the WSW away from Terceira Island (Fig. 5D). The velocities of sites located in the NW and SE sectors of the island differ by ~1 mm/yr (Fig. 5A), indicating that slow intra-island deformation occurs (Mendes et al., 2013). In Section 5.2, we use velocities from S. Jorge to test the hypothesis that the Terceira Rift accommodates all Nubia–Eurasia motion.

Relative to the Nubia plate, sites in the NW sector of S. Jorge move 2–2.5 mm/yr toward the east, and sites in the SE sector move 1.5–2 mm/yr toward the SE (not shown), consistent with results reported by Mendes et al. (2013). The island therefore does not move with the Nubia plate, a conclusion that is independent of which sector of the island best represents its long-term motion. We refer readers to Mendes et al. (2013) for a more complete description of their GPS velocities and interpretation of the velocity field in the context of the volcanotectonic setting of the island.

3.5. Pico and Faial islands

Pico and Faial islands, which occupy the Pico/Faial volcanic ridge, move WSW away from the Eurasia plate (Fig. 5C) at rates of 2–4 mm/yr (Fig. 5D). Relative to the Eurasia plate, the velocities of the 8 Pico Island sites and 4 sites on the eastern half of Faial Island average 3.5 ± 0.5 mm/yr (2-σ), approximately 80% of the Nubia–Eurasia plate rate (Fig. 5D) and ~1 mm/yr faster than sites on S. Jorge Island. To test for significant motion of the Pico/Faial volcanic ridge relative to the Nubia plate, we repeated the statistical test for an additional plate using the 49 Nubia plate site velocities and 12 velocities from Pico and eastern Faial islands. The differ-

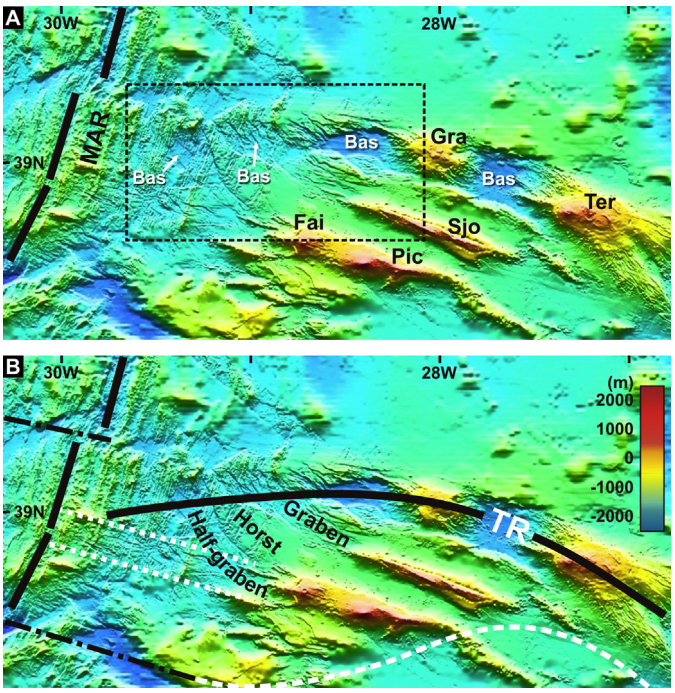

Fig. 6. Bathymetry of the western end of the TR, in its junction with the MAR axis. Black heavy lines – ridge axes (MAR and TR). Long-dashed white line – northern shoulder of the TR. Dashed white line – southern limit of deformation and seismicity, here proposed as the southern boundary of the diffuse Nubia–Eurasia boundary, based on extension-related structures, seismicity and GPS measurements. Dash-dot lines – transform faults. Dotted lines mark the limits of a strip of concentrated N110°normal faulting. Bas – basins. Lighting from N. Dashed rectangle marks the region shown in Fig. 7. JPG image made available by Joaquim Luis (http://w3.ualg.pt/~jluis/).

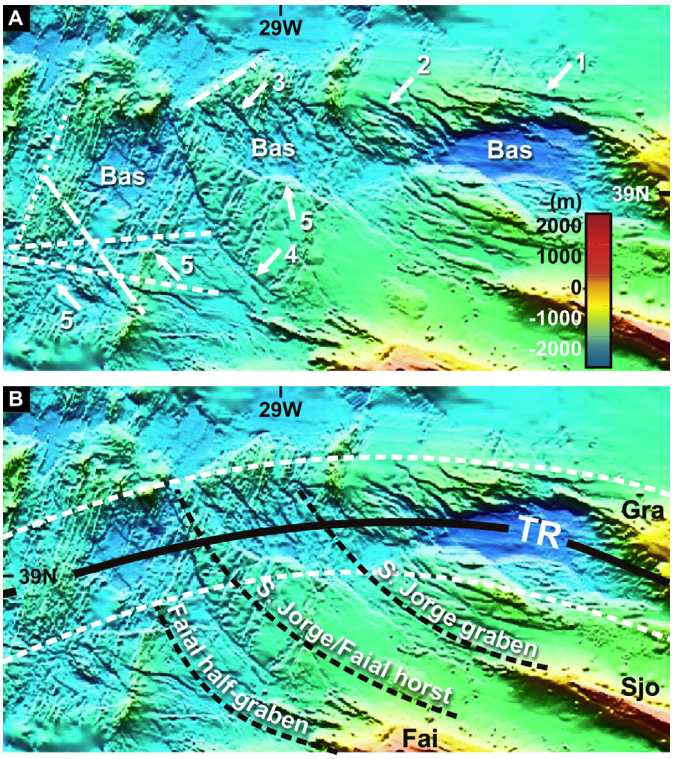

Fig. 7. Close up of Fig. 6, as marked by the dashed rectangle. Note: (1) the gradual change in orientation of faults marked 1 to 3 in A; (2) the main structural orientations – dominant faults striking N80–110° (dashed white lines in A) and N150° (long-dashed white line in A), N60° faults (e.g. dash-dotted line in A) bounding some basins, and MAR linear fabric (dotted line in A); (3) the curved graben-horst outlined in B; (4) suggested boundaries of western termination of the TR, with deformation mostly by en échelon normal faulting and formation of basins (Bas) (dashed thick white line in B); (5) the similarity between the shape and orientation of the two basins marked Bas in black. Full black line in B – axis of the TR. Lighting from N.

ence in the least-squares fits for models that fit these two velocity subsets with one or two angular velocities is significant at a confidence level much greater than 99%, with $F = 23.7$ for 3 versus 116 degrees of freedom. We conclude that the Pico/Faial volcanic ridge moves relative to the Nubia plate (also see black arrow in Fig. 5A).

Given the similarity of the velocities of stations on Pico Island and the eastern half of Faial Island, we inverted them together to construct a frame of reference tied to the Faial/Pico volcanic ridge. The resulting velocity field (Fig. 5a) clearly shows ~1 mm/yr of NE-directed extension between the Faial/Pico and S. Jorge volcanic ridges. It also illustrates that sites in western Faial move relative to the volcanic ridge farther east. Although the reasons for this movement are unclear, their proximity to the 1957/58 eruption that added 1.5 km^2 to western Faial suggests a volcanic origin for the anomalous GPS velocities.

4. Structural and seismic data

4.1. Structural data

In the mostly submarine Azores region, detailed bathymetric maps are useful for interpreting recent seafloor deformation because faults are abundant, young (as evidenced by the abundance of seismic activity), are clearly revealed due to low sedimentation rates, and are easily recognized due to their significant vertical offsets. We thus invest significant effort below in interpreting the available bathymetry to provide a framework for understanding both the regional-scale deformation at the western end of the Nubia–Eurasia boundary and for interpreting the GPS velocities.

The Nubia–Eurasia plate boundary in the Azores is defined by the following series of features, which are described below and illustrated in Figs. 6 and 7.

(1) The Terceira Rift is a prominent sigmoidal and deep graben, which extends several hundred km from the MAR axis (at ca. 39°N, 29.89°W) to the East Formigas Basin near the junction with the Azores–Gibraltar Fault (Figs. 1 and 6). The rift is filled at regular spaces (ca. 80 km) by concentrated volcanism forming islands or seamounts that rise near to the sea surface.
(2) A curved graben-horst structure (Figs. 6B and 7B), west of Faial and S. Jorge islands, bounded by faults that gradually change strike from azimuth N160° in the N to azimuth N110° in the S (marked 4 in Fig. 7A). The grabens are here called S. Jorge graben and Faial half-graben, and the intervening tectonic high here called the S. Jorge–Faial horst (Fig. 7B). The main fault scarps bounding these grabens are as high as 200 m.
(3) Smaller trapezoidal basins bounded on all four sides by faults (marked Bas in Figs. 6 and 7). These basins occur along two lineaments, mostly between Graciosa Island and MAR axis.
(4) Faults arranged en échelon in an ENE-WSW band running from the N edge of the West Graciosa Basin to close to the MAR axis (marked 1, 2 and 3 in Fig. 7A); fault strike varies gradually from N100° in the E to N145° in the W. From their bathymetric expressions, the faults appear to be normal faults dipping to W (mostly) and E, thus defining grabens (e.g. the S. Jorge graben), half grabens (e.g. the Faial half-graben) and horsts (e.g. the S. Jorge/Faial horst) (Figs. 6 and 7).
(5) Faults with different trends, mostly concentrated along the N110° (white dashed lines in Figs. 6 and 7), N150° long-dashed line) and N60° (dash-dotted line) directions.
(6) Close to the MAR axis, fractures and faults are mostly perpendicular to the ridge axis (parallel to transforms), and thus

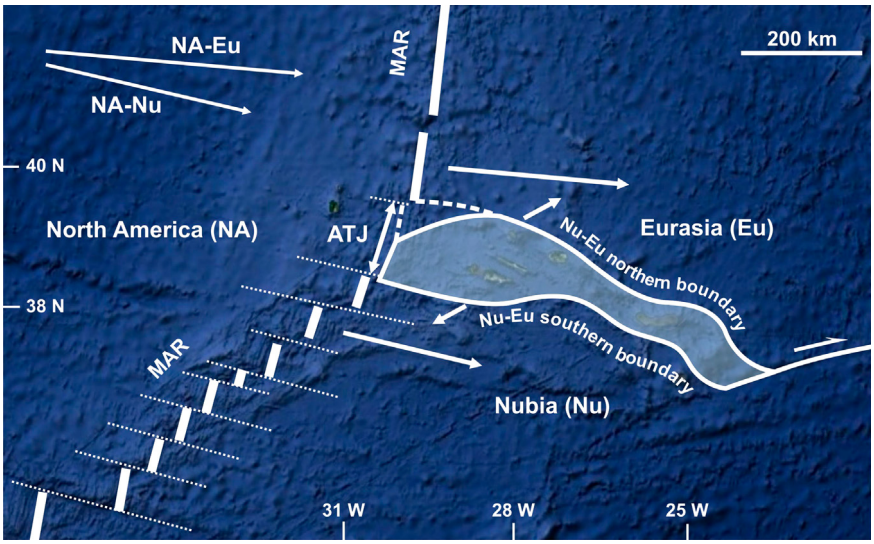

Fig. 8. Proposed Nu–Eu plate boundary in the Azores. Shadowed area is the diffuse plate boundary inferred from GPS, bathymetric, structural and seismic data. Inset on top left corner shows kinematics of the Nubia and Eurasia lithospheric plates (DeMets et al., 2010). Dotted lines represent transform faults. Background image is from Google.

strike between N80° and N110°. These fractures/faults are disrupted by the N150° aults (marked 5 in Fig. 7).

(7) Linear volcanic ridges that seem to have grown mostly along N110° fractures, at least during the last 400 kyr (Hildenbrand et al., 2008, 2012a, 2012b, 2013). The S. Jorge Island lies on top of the S. Jorge graben, and the Pico–Faial ridge sits on top of the northern edge of the Faial half graben.

(8) Strip of N110° normal faulting stretching from the MAR axis to the Faial-Pico ridge. This concentration of normal faulting can be the result of MAR change in strike at around 39°N (Fig. 6b).

Detailed bathymetric images of some of the major structures described above, as well as detailed bathymetry around some of the islands studied in the present work, can be found in Mitchell et al. (2008, 2012), Quartau and Mitchell (2013), Quartau et al. (2012), Stretch et al. (2006) and Tempera et al. (2012). Madeira and Brum da Silveira (2003) reported on the inland expression of some of the faults described above.

4.2. Seismic data

Earthquake epicentres and focal mechanisms offer useful information about the local tectonics (Fig. 2). In general, the widespread seismicity is consistent with the hypothesis that deformation in the study area is distributed rather than concentrated along a well-defined plate boundary. For example, earthquakes located west of the Pico–Faial ridge are most likely the result of extension within the Faial half-graben (Figs. 7 and 8), and earthquakes west of S. Jorge are probably related to opening across the S. Jorge graben (Figs. 7 and 8). Both support the GPS evidence for distributed oblique extension between Terceira, S. Jorge, and Pico/Faial islands.

The few available earthquake focal mechanisms (Fig. 2A) define two possible fault planes, N100–120° and N140–160°, both coinciding with the dominant orientations of faults in the bathymetry (Figs. 7 and 8). Analyses of body waves and aftershocks of the $M = 7.2$ 1980 earthquake (Hirn et al., 1980; Grimison and Chen, 1988; Borges et al., 2007) suggest that it ruptured an N150°-striking fault, thereby implying sinistral strike-slip motion (Fig. 2A). From body-wave modeling, Borges et al. (2007) also proposed that the $M_w = 6.2$ 1998 Faial Island earthquake ruptured a N150°-striking fault. Matias et al. (2007) also suggested that the 1998 Faial earthquake was a shallow (<5 km depth) sinistral strike-slip earthquake on a N150°-striking fault. In contrast, Fernandes et al. (2002) were unable to identify the rupture plane of the 1998 Faial earthquake based on ground motion and numerical modeling.

Assuming that both of these strike-slip earthquakes ruptured faults that strike ~N150°, the faults are oriented at a high angle to the Nubia–Eurasia plate direction (Fig. 4B) and thus cannot accommodate Nubia–Eurasia motion by themselves. By inference, other faults must accommodate some of the plate movement. Within the study area, the tensional axes for the eight strike-slip and normal-faulting earthquakes between 29.5°W and 27.5°W in Fig. 2A are nearly all oriented NNE–SSW. The average T axis orientation for these eight earthquakes, N22°E (indicated by double-headed arrows in Figs. 2 and 5B), is perpendicular to the volcanic ridges occupied by S. Jorge and Pico and Faial islands, which trend N110°E. The direction of principal instantaneous extensional strain indicated by the earthquakes is thus consistent with (i.e. orthogonal to) the trends of the main volcanic ridges. The average T axis is however oriented 45° and 70° counter clockwise from the Nubia–Eurasia directions predicted by the MORVEL and GPS angular velocities for Nubia–Eurasia motion, respectively.

The discrepancy between the predicted plate motion and the seismic deformation can be reconciled by one or more of the following: (1) The earthquakes recorded during the past few decades may not fully characterize the long-term deformation in the study area given the slow deformation rates, (2) crustal extension south of the Terceira Rift may be accompanied by aseismic block rotations, and (3) partitioning of the plate motion could occur, possibly between structures in the Terceira Rift and the volcanic ridges SW of Terceira Island.

In summary, well-constrained, high-magnitude earthquakes summarized in Borges et al. (2007) and augmented by more recent earthquakes (Fig. 2A) indicate that earthquakes are dominantly normal-faulting or strike slip. At least some of the latter record sinistral strike-slip motion along faults trending N150°, at high angle to the predicted plate motion. The bulk of the evidence suggests that deformation is diffuse and may include either block rotations south of the Terceira Rift or partitioning of distinctly different motions within different domains of the study area in order to accommodate the predicted motion between Nubia and Eurasia.

5. Discussion

5.1. GPS constraints on inter-island motions

A comparison of the GPS velocities of Pico, Faial, S. Jorge and Terceira islands with the Nubia–Eurasia velocity in the Azores region (ca. 4.5 mm/yr, DeMets et al., 2010) shows that the islands belong to neither the Eurasia nor Nubia plates. Relative to Eurasia, Terceira moves ca. 2 mm/yr to the west, a likely result of its location within the Terceira Rift. S. Jorge, which lies on the southern shoulder of the Terceira Rift WSW of Terceira Island, moves WSW at ca. 3 mm/yr relative to the Eurasia plate. S. Jorge thus moves away from Terceira at ca. 1 mm/yr, as the result of aggregate opening across the Terceira Rift and the S. Jorge graben (Figs. 5 and 8). Faial and Pico move to the WSW away from Eurasia at ca. 3.5 mm/yr faster than both S. Jorge and Terceira islands, and consistent with distributed oblique divergence between the NE edge of the Terceira Rift and Pico/Faial islands.

5.2. Is the Terceira Rift the Nubia–Eurasia plate boundary?

The new GPS velocities permit a strong test of the hypothesis that the Terceira Rift is the sole plate boundary structure. Since Terceira Island is located within the rift, GPS velocities from Terceira Island cannot be used for the test. Rather, GPS velocities from S. Jorge, the nearest island WSW of the Terceira Rift, must be used. As is shown in Fig. 5D, sites on S. Jorge Island move to the WSW from 2 to 4 mm/yr and average 2.7 ± 0.7 mm/yr, ca. 60% of the Nubia–Eurasia plate rate (Fig. 5D). A statistical test for significant motion between S. Jorge and the Nubia plate passes with high probability ($\gg$99% confidence level). The hypothesis that all Nubia–Eurasia motion is accommodated by the Terceira Rift, as suggested by Vogt and Jung (2004), is thus inconsistent with the current GPS data. The available data instead suggest a lower bound of 2 ± 1 mm/yr of extension across the Terceira Rift (Fig. 5D), and an upper bound of 2.7 ± 0.7 mm/yr based on GPS sites motions on S. Jorge Island and the unlikely assumption that no extension occurs across the S. Jorge graben between S. Jorge and Terceira islands.

5.3. Implications for Nubia–Eurasia plate boundary geometry

Taken together, the GPS, bathymetric, and seismic data define the volcanic and tectonic framework of the western end of the Nubia–Eurasia plate boundary. The central question of our analysis is whether these data favor a model in which deformation is distributed across a wide zone encompassing the northern half of the Azores plateau or a model in which most or all of the plate boundary slip is confined to a narrow zone. As described above, the GPS observations reject a narrow boundary that coincides with the prominent Terceira Rift. The existence of numerous ESE–WNW-trending faults that cross-cut the young abyssal hill fabric of the MAR between 38.4°N and 39.3°N (Figs. 7 and 8), within what would otherwise be defined as the Azores microplate, strongly argues against a narrow-boundary (or rigid microplate) model. The ESE-WNW-striking faults appear to connect the MAR to the zone of distributed oblique extension defined by Terceira, S. Jorge, Faial, and Pico islands, and thus define a diffuse boundary between the Nubia and Eurasia plates. The distributed seismicity in the same area as these crosscutting faults (Fig. 2B) constitutes additional evidence for distributed deformation, although the epicentral locations are too imprecise to strictly assign the earthquakes to well identified cross-cutting faults.

If the Nubia–Eurasia plate boundary were narrow at the triple junction, seafloor spreading rates would change suddenly along the MAR immediately north and south of the triple junction. The spreading rates instead change gradually (see Fig. 22 in DeMets et al., 2010), indicating there is either a rigid or nearly rigid Azores microplate moving independently of Nubia and Eurasia east of the MAR axis between ~38°N and 39.5°N, or that distributed deformation occurs across a ~140-km-wide zone east of the MAR axis. The evidence outlined in the previous paragraphs clearly favors the latter possibility.

The pattern of GPS velocities and horst-and-graben morphology between Terceira, S. Jorge, and Pico/Faial islands (Figs. 5, 7, 8) offer further evidence for an accommodation of Nubia–Eurasia motion across a wide rather than narrow zone. The GPS velocities clearly show that WSW-directed extension (relative to the Eurasia plate) is accommodated by a combination of opening across the Terceira Rift and smaller scale grabens WSW of the rift (Fig. 5). GPS site velocities only begin to reach the full Nubia–Eurasia plate rate at a distance greater than 140 km south of the Terceira Rift. The GPS velocities clearly show that the extension across the Terceira Rift does not account for all of the plate motion, hence the Eurasia-Nubia plate boundary is not discrete. Oblique extension is instead distributed across a plate boundary at least 140 km wide spanning the islands of Terceira, S. Jorge and Pico/Faial (Fig. 8).

Based on the GPS velocities, seismic data, and seafloor morphology, we hypothesize that Nubia–Eurasia plate motion in the Azores is accommodated by a wide zone of oblique extensional deformation limited by the MAR axis in the west, the northern shoulder of the Terceira Rift in the north, and in the south, by a line that connects the MAR axis at 38.4°N, 30.5°W to the East Formigas Basin (36.9°N, 23.6°W), passing south of the Pico–Faial ridge and SE of the S. Jorge Island. The southern boundary is defined by the transition from the concentration of faults and earthquakes in the north to an area in the south where there are few signs of active deformation.

The above interpretation implies that the Azores triple “point” is better thought of as a diffuse triple junction.

5.4. Limitations due to elastic effects of locked faults and volcanic processes

At least two factors limit our interpretations of the tectonic implications of the GPS velocity field. First, the influences of volcanic processes and mass wasting on the GPS velocity field are poorly understood, but may be potentially important on an island-by-island basis (Mendes et al., 2013; Miranda et al., 2012). Second, widespread earthquake activity in the Azores islands (Borges et al., 2007 and Fig. 2B) clearly suggests there are multiple locked faults within our study area. Interseismic elastic deformation associated with these faults and possible viscoelastic effects from large earthquakes during the past few decades both affect the GPS velocity field in the study area to an unknown degree. Depending on the spacing and geometry of the active faults, their elastic effects may overlap and give rise to a GPS velocity field more characteristic of continuous than discrete deformation.

Unfortunately, estimating these location-dependent elastic effects via forward modeling requires knowledge of the principal active faults and their long-term slip rates. Neither are well known – historic earthquakes near Pico, Faial, S. Jorge and Terceira islands are dominantly strike-slip events on submarine faults distributed within the study area (Fig. 2A and Borges et al., 2007). Given the uncertainties in modeling the elastic deformation and the sensitivity of the predicted elastic deformation to the input parameters, we elected not to model those effects.

Inverse modeling of the GPS velocity field and other kinematic constraints such as earthquake focal mechanisms could conceivably be used to discriminate between rigid or semi-rigid microplate and continuum or distributed deformation models for this region (e.g.

McCaffrey, 2002; Meade and Loveless, 2009). Such models however require information about the locations and geometry of the principal block-bounding faults, which, as noted above, remain poorly known for the study area.

6. Conclusions

From newly determined GPS velocities from the Azores archipelago, and Eurasia and Nubia plates, we find that oblique WSW-ENE extension between the Nubia and Eurasia plates is accommodated across a series of horsts and grabens that include the Pico/Faial volcanic ridge, which moves mostly with Nubia, Terceira Island, which moves mostly with Eurasia, and S. Jorge Island, whose motion is intermediate between that of Nubia and Eurasia. From these observations and existing bathymetric and seismic data, we conclude the following:

1. The Nubia–Eurasia plate boundary at the longitude of the Azores is diffuse, comprising a ca. 140-km-wide zone of deformation shown in Fig. 8.
2. The opening rate in the Terceira Rift is much smaller than previously thought, because it does not take up the whole deformation imposed by the motions of Nubia and Eurasia.
3. The Azores Triple Junction is diffuse, stretching along the MAR axis between 38.3°N, 30.3°W and 39.4°N, 29.7°W, where spreading rates decrease gradually from ca. 22.5 mm/yr N of 40°N to 19.5 mm/yr S of 38°N.
4. The new data do not require the existence of an independent Azores microplate.

Acknowledgements

This is a contribution to Project MEGAHazards (PTDC/CTE-GIX/108149/2008) funded by FCT Portugal. Funding for C. DeMets was provided by U.S. National Science Foundation grant OCE-0926274. We are grateful to colleague Joaquim Luis (http://w3.ualg.pt/~jluis/) for kindly offering the higher resolution image of the Azores bathymetry. We thank Neil Mitchell and an anonymous reviewer for comments that helped improve the quality of this manuscript.

References

Altamimi, Z., Collilieux, X., Legrand, J., Garayt, B., Boucher, C., 2007. ITRF2005: A new release of the international terrestrial reference frame based on time series of station positions and Earth orientation parameters. J. Geophys. Res. 112, B09401, http://dx.doi.org/10.1029/2007JB004949.

Altamimi, Z., Collilieux, X., Metivier, L., 2011. ITRF2008: An improved solution of the international terrestrial reference frame. J. Geod. 8, 457–473.

Argus, D.F., 2007. Defining the translational velocity of the reference frame of Earth. Geophys. J. Int. 169, 830–838.

Argus, D.F., Gordon, R.G., Heflin, M.B., Ma, C., Eanes, R., Willis, P., Peltier, W.R., Owen, S.E., 2010. The angular velocities of the plates and the velocity of Earth's centre from space geodesy. Geophys. J. Int. 180, 913–960.

Böhm, J., Werl, B., Schuh, H., 2006. Troposphere mapping functions for GPS and very long baseline interferometry from European Centre Medium-Range Weather Forecasts operational analysis data. J. Geophys. Res. 111, B02406, http://dx.doi.org/10.1029/2005JB003629.

Borges, J.F., Bezzeghoud, M., Buforn, E., Pro, C., Fitas, A., 2007. The 1980, 1997 and 1998 Azores earthquakes and some seismo-tectonic implications. Tectonophysics 435, 37–54.

Calais, E., DeMets, C., Nocquet, J.-M., 2003. Evidence for a post-3.16 Ma change in Nubia–Eurasia–North America plate motions? Earth Planet. Sci. Lett. 216, 81–92.

Catalão, J., Miranda, J.M., Lourenço, N., 2006. Deformation associated with the Faial (Capelinhos) 1956 eruption. Inferences from 1937–1997 geodetic measurements. J. Volcanol. Geotherm. Res. 155, 151–163.

DeMets, C., Gordon, R.G., Argus, D.F., 2010. Geologically current plate motions. Geophys. J. Int. 181, 1–80.

Dong, D., Herring, T.A., King, R.W., 1998. Estimating regional deformation from a combination of space and terrestrial geodetic data. J. Geod. 72, 200–214.

Dziewonski, A.M., Chou, T.-A., Woodhouse, J.H., 1981. Determination of earthquake source parameters from waveform data for studies of global and regional seismicity. J. Geophys. Res. 86, 2825–2852.

Ekstrom, G., Nettles, M., Dziewonski, A.M., 2012. The global CMT project 2004–2010: Centroid-moment tensors for 13,017 earthquakes. Phys. Earth Planet. Inter. 200–201, 1–9.

Fernandes, R.M.S., Miranda, J.M., Catalão, J., Luis, J.F., Bastos, L., Ambrosius, B.A.C., 2002. Coseismic displacements of the MW = 6.1, July 9, 1998, Faial earthquake (Azores, North Atlantic). Geophys. Res. Lett. 29, 1–4.

Fernandes, R.M.S., Bastos, L., Miranda, J.M., Lourenço, N., Ambrosius, B.A.C., Noomen, R., Simons, W., 2006. Defining the plate boundaries in the Azores region. J. Volcanol. Geotherm. Res. 156, 1–9.

Grimison, N., Chen, W., 1988. The Azores–Gibraltar plate boundary: focal mechanisms, depths of earthquakes and their tectonic implications. J. Geophys. Res. 91, 2029–2047.

Hirn, A., Haessler, J., Hoang Trong, P., Wittlinger, G., MendesVictor, L., 1980. Aftershock sequence of the January 1st, 1980 earthquake and present-day tectonics in the Azores. Geophys. Res. Lett. 7, 501–504.

Herring, T.A., King, R.W., McClusky, S.C., 2010. GLOBK Reference Manual Release 10.4. Department of Earth, Atmospheric, and Planetary Sciences, Massachusetts Institute of Technology, Cambridge.

Hildenbrand, A., Madureira, P., Marques, F.O., Cruz, I., Henry, B., Silva, P., 2008. Multistage evolution of a sub-aerial volcanic ridge over the last 1.3 Myr: S. Jorge Island, Azores Triple Junction. Earth Planet. Sci. Lett. 273, 289–298.

Hildenbrand, A., Marques, F.O., Fernandes, J.C.C.C., Catita, C.M.S., Costa, A.C.G., 2012a. Large-scale active slump of the southeastern flank of Pico Island, Azores. Geology 40, 939–942.

Hildenbrand, A., Marques, F.O., Costa, A.C.G., Sibrant, A.L.R., Silva, P.M.F., Henry, B., Miranda, J.M., Madureira, P., 2012b. Reconstructing the architectural evolution of volcanic islands from combined K/Ar, morphologic, tectonic, and magnetic data: the Faial Island example (Azores). J. Volcanol. Geotherm. Res. 241–242, 39–48.

Hildenbrand, A., Marques, F.O., Costa, A.C.G., Sibrant, A.L.R., Silva, P.M.F., Henry, B., Miranda, J.M., Madureira, P., 2013. Reply to the comment by Quartau and Mitchell on "Reconstructing the architectural evolution of volcanic islands from combined K/Ar, morphologic, tectonic, and magnetic data: The Faial Island example (Azores)". J. Volcanol. Geotherm. Res. 241–242, 39–48, by Hildenbrand et al., 2012. J. Volcanol. Geotherm. Res. 255, 127–130.

Krause, D.C., Watkins, N.D., 1970. North Atlantic crustal generation in the vicinity the Azores. Geophys. J. R. Astron. Soc. 19, 261–283.

Lourenço, N., Luis, J.F., Miranda, J.M., Ribeiro, A., Mendes Victor, L.A., Madeira, J., Needham, H.D., 1998. Morpho-tectonic analysis of the Azores Volcanic Plateau from a new bathymetric compilation of the area. Mar. Geophys. Res. 20, 141–156.

Luis, J.F., Miranda, J.M., 2008. Reevaluation of magnetic chrons in the North Atlantic between 35°N and 47°N: Implications for the formation of the Azores Triple Junction and associated plateau. J. Geophys. Res. 113, B10105, http://dx.doi.org/10.1029/2007JB005573.

Luis, J.F., Miranda, J.M., Galdeano, A., Patriat, P., Rossignol, J.C., Mendes Victor, L.A., 1994. The Azores Triple Junction evolution since 10 Ma from an aeromagnetic survey of the Mid-Atlantic Ridge. Earth Planet. Sci. Lett. 125, 439–459.

Lyard, F., Lefèvre, F., Letellier, T., Francis, O., 2006. Modelling the global ocean tides: a modern insight from FES2004. Ocean Dyn. 56, 394–415.

Madeira, J., Brum da Silveira, A., 2003. Active tectonics and first paleoseismological results in Faial, Pico and S. Jorge islands (Azores, Portugal). Ann. Geophys. 46, 733–761.

Madeira, J., Ribeiro, A., 1990. Geodynamic models for the Azores Triple Junction: a contribution from tectonics. Tectonophysics 184, 405–415.

Mao, A., Harrison, C.G.A., Dixon, T.H., 1999. Noise in GPS coordinate time series. J. Geophys. Res. 104, 2797–2816.

Marquez-Azua, B., DeMets, C., 2003. Crustal velocity field of Mexico from continuous GPS measurements, 1993 to June, 2001: Implications for the neotectonics of Mexico. J. Geophys. Res. 108, http://dx.doi.org/10.1029/2002JB002241.

Matias, L., Dias, N., Morais, I., Vales, D., Carrilho, F., Madeira, J., Gaspar, J., Senos, L., Silveira, A., 2007. The 9th of July 1998 Faial Island (Azores, North Atlantic) seismic sequence. J. Seismol. 11, 275–298.

McCaffrey, R., 2002. Crustal block rotations and plate coupling. In: Stein, S., Freymueller, J. (Eds.), Plate Boundary Zones. In: Geodynamics Series, vol. 30. American Geophysical Union, Washington, pp. 101–122.

Meade, B.J., Loveless, J.P., 2009. Block modeling with connected fault-network geometries and a linear elastic coupling estimator in spherical coordinates. Bull. Seismol. Soc. Am. 99, 3124–3239.

Mendes, V.B., Madeira, J., Brum da Silveira, A., Trota, A., Elosegui, P., Pagarete, J., 2013. Present-day deformation in São Jorge Island, Azores, from episodic GPS measurements (2001–2011). Adv. Space Res. 51, 1581–1592.

Miranda, J.M., Navarro, A., Catalão, J., Fernandes, R.M.S., 2012. Surface displacement field at Terceira Island deduced from repeated GPS measurements. J. Volcanol. Geotherm. Res. 217, 1–7.

Miranda, J.M., Luis, J.F., Abreu, I., Mendes Victor, L.A., Galdeano, Q., Rossignol, J.C., 1991. Tectonic framework of the Azores Triple Junction. Geophys. Res. Lett. 18, 1421–1424.

Mitchell, N.C., Beier, C., Rosin, P., Quartau, R., Tempera, F., 2008. Lava penetrating water: Submarine lava flows around the coasts of Pico Island, Azores. Geochem. Geophys. Geosyst. 9, http://dx.doi.org/10.1029/2007GC001725.

Mitchell, N.C., Stretch, R., Oppenheimer, C., Kay, D., Beier, C., 2012. Cone morphologies associated with shallow marine eruptions: east Pico Island, Azores. Bull. Volcanol. 74, 2289–2300.

Navarro, A., Catalão, J., Miranda, J.M., Fernandes, R.M.S., 2003. Estimation of the Terceira Island (Azores) main strain rates from GPS data. Earth Planets Space 55, 637–642.

Nocquet, J.-M., Calais, E., Parsons, B., 2005. Geodetic constraints on glacial isostatic adjustment in Europe. Geophys. Res. Lett. 32, L06308, http://dx.doi.org/10.1029/2004GL022174.

Petit, G., Luzum, B., 2010. IERS conventions, 2010. IERS Technical Note; No. 36. Verlag des Bundesamts fur Kartographie und Geodasie, Frankfurt am Main.

Quartau, R., Mitchell, N.C., 2013. Comment on "Reconstructing the architectural evolution of volcanic Islands from combined K/Ar, morphologic, tectonic, and magnetic data: The Faial Island example (Azores)". by Hildenbrand et al. 2012. J. Volcanol. Geotherm. Res. 241–242 (2012) 39–48. J. Volcanol. Geotherm. Res. 255, 124–126.

Quartau, R., Tempera, F., Mitchell, N.C., Pinheiro, L.M., Duarte, H., Brito, P.O., Bates, C.R., Monteiro, J.H., 2012. Morphology of Faial Island's shelf: The results of volcanic, erosional, depositional and mass-wasting processes. Geochem. Geophys. Geosyst. 13, http://dx.doi.org/10.1029/2011GC003987.

Saastamoinen, J., 1972a. Contributions to the theory of atmospheric refraction. Bull. Géod. 105, 279–298, I part.

Saastamoinen, J., 1972b. Contributions to the theory of atmospheric refraction. Bull. Géod. 106, 383–397, II part.

Saastamoinen, J., 1973. Contributions to the theory of atmospheric refraction. Bull. Géod. 107, 13–34, III part.

Searle, R., 1980. Tectonic pattern of the Azores spreading centre and triple junction. Earth Planet. Sci. Lett. 51, 415–434.

Stein, S., Gordon, R.G., 1984. Statistical tests of additional plate boundaries from plate motion inversions. Earth Planet. Sci. Lett. 69, 401–412.

Stretch, R., Mitchell, N.C., Portaro, R.A., 2006. A morphometric analysis of the submarine volcanic ridge of Pico Island. J. Volcanol. Geotherm. Res. 156, 35–54.

Tempera, F., Giacomello, E., Mitchell, N.C., Campos, A.S., Henriques, A.B., Martins, A., Bashmachnikov, I., Mendonça, A., Morato, T., Colaço, A., Porteiro, F.M., Catarino, D., Gonçalves, J., Pinho, M.R., Isidro, E.J., Santos, R.S., Menezes, G., 2012. Mapping the Condor seamount seafloor environment and associated biological assemblages (Azores, NE Atlantic). In: Harris, P.T., et al. (Eds.), Seafloor Geomorphology as Benthic Habitat: Geohab Atlas of Seafloor Geomorphic Features and Benthic Habitats. Elsevier, London, pp. 807–818.

Vogt, P.R., Jung, W.Y., 2004. The Terceira Rift as hyper-slow, hotspot-dominated oblique spreading axis: A comparison with other slow-spreading plate boundaries. Earth Planet. Sci. Lett. 218, 77–90.

Zumberge, J.F., Heflin, M.B., Jefferson, D.C., Watkins, M.M., Webb, F.H., 1997. Precise point positioning for the efficient and robust analysis of GPS data from large networks. J. Geophys. Res. 102, 5005–5017.